Available online at www.sciencedirect.com
ScienceDirect
Journal of Hazardous Materials 152 (2008) 1098–1107
Journal of Hazardous Materials
www.elsevier.com/locate/jhazmat

Mass transfer of VOCs in laboratory-scale air sparging tank

Keh-Ping Chao [a,*], Say Kee Ong [b], Mei-Chuan Huang [a,c]

[a] Department of Occupational Safety & Health, China Medical University, 91 Hsueh-Shih Rd., Taichung 40402, Taiwan, ROC
[b] Department of Civil, Construction & Environmental Engineering, Iowa State University, Ames, USA
[c] Institute of Engineering Science & Technology, National Kaohsiung First University of Science & Technology, Taiwan, ROC

Received 28 March 2007; received in revised form 26 July 2007; accepted 26 July 2007
Available online 31 July 2007

Abstract

Volatilization of VOCs was investigated using a 55-gal laboratory-scale model in which air sparging experiments were conducted with a vertical air injection well. In addition, X-ray imaging of an air sparging sand box showed air flows were in the form of air bubbles or channels depending on the size of the porous media. Air–water mass transfer was quantified using the air–water mass transfer coefficient which was determined by fitting the experimental data to a two-zone model. The two-zone model is a one-dimensional lumped model that accounts for the effects of air flow type and diffusion of VOCs in the aqueous phase. The experimental air–water mass transfer coefficients, $K_G a$, obtained from this study ranged from 10^{-2} to 10^{-3} 1/min. From a correlation analysis, the air–water mass transfer coefficient was found to be directly proportional to the air flow rate and the mean particle size of soil but inversely proportional to Henry's constant. The correlation results implied that the air–water mass transfer coefficient was strongly affected by the size of porous media and the air flow rates.

Keywords: Volatilization; VOCs; Air sparging; Air–water mass transfer

1. Introduction

Accidental releases of petroleum products and volatile organic compounds (VOCs) have resulted in gross contamination of soils and groundwater. Several remedial technologies have been developed to treat contaminated soils and groundwater. One of the in situ remedial technologies, air sparging, employs contaminant-free air to volatilize VOCs from the groundwater into the air phase. Air sparging creates a transient air-filled porosity by displacing water in the soil matrix, with the forced air traveling through the saturated zone. The volatilized VOCs carried by the air stream are subsequently transported into the unsaturated zone where the VOC-contaminated air is captured by soil vapor extraction (SVE) systems. In addition to the physical removal of VOCs by volatilization, aerobic biodegradation of contaminants by indigenous microorganisms may be enhanced due to the presence of a higher dissolved oxygen concentration in groundwater. However, volatilization is the primary mass removal mechanism for air sparging systems [1].

The effectiveness of an air sparging system to volatilize VOCs from the subsurface mainly depends on the nature of air flow in saturated porous media, chemical properties of VOCs, and mass transfer mechanisms. Under air sparging conditions, air flow in saturated porous media is highly complex and will depend on air injection conditions and the properties of porous media. Because the subsurface at contaminated sites cannot be observed, several laboratory-scale air sparging experiments have contributed insights into the air flow geometry and patterns. Experiments have been conducted using a transparent tank where air flow can be observed directly [2], or by colorimetric visualization methods using iron filings [3].

Several researchers have indicated that injection of air into the aquifer created air bubbles which moved horizontally and vertically through the groundwater [4]. In their description an air sparging system may be treated like a crude air stripper in the subsurface with the soil acting as the packing. On the other hand, Hinchee [5] reported that it appears doubtful that air bubbles would form and migrate in a sandy aquifer, except perhaps in highly permeable gravel aquifers. The injected air would travel as slugs of air pockets through preferential pathways in the aquifer. Pankow et al. [6] indicated that the injected air traveled through the aquifer either in channel form or in bubble form.

* Corresponding author. Tel.: +886 4 22053366x6205; fax: +886 4 22070500.
E-mail address: kpchao@mail.cmu.edu.tw (K.-P. Chao).

0304-3894/$ – see front matter © 2007 Elsevier B.V. All rights reserved.
doi:10.1016/j.jhazmat.2007.07.087

Nomenclature

A	interfacial surface area between air and water phases (L^2)
A_s	cross section area of the sparging tank (L^2), i.e. 71.2 cm^2
C_a	average VOC concentrations in the air phase ($M L^{-3}$)
C_a^o	initial VOC concentrations in the sparged air ($M L^{-3}$)
$C^o_{a,experimental}$	VOC air concentration as initializing the sparging experiment (ML^{-3})
C_{wm}	average VOC concentration in water of the MTZ ($M L^{-3}$)
C^o_{wm}	initial average VOC concentration in water of the MTZ ($M L^{-3}$)
d_{50}	mean particle size of the porous media (L)
d_m	mean grain size of medium sand (L), i.e. 0.05 cm
d_o	normalized mean particle size (dimensionless)
D_G	molecular diffusivity of VOC in the air phase ($L^2 T^{-1}$)
D_L	molecular diffusivity of VOC in the liquid phase ($L^2 T^{-1}$)
f_{oc}	organic carbon content (%)
F	volume fraction of MTZ to the total saturated porous media (dimensionless)
g	gravitational acceleration ($L T^{-2}$)
H	Henry's constant (dimensionless)
J	rate of VOC transfer across the air–water interface ($M T^{-1}$)
K_G	overall gas-phase mass transfer coefficient ($L T^{-1}$)
K_Ga	air–water mass transfer coefficient (T^{-1})
K_GA	mass transfer coefficient ($L^3 T^{-1}$)
k_La	liquid-phase mass transfer coefficient (T^{-1})
K_{oc}	organic carbon partitioning coefficient (L^3M^{-1})
K_p	soil–water partition coefficient ($L^3 M^{-1}$)
M^o	initial mass of VOC in the sparging tank (M)
M_s	total mass of porous media (M)
MTZ	mass transfer zone
Pe	Peclet number (dimensionless)
Q	injected air flow rate ($L^3 T^{-1}$)
Sh	Sherwood number (dimensionless)
V	volume of aquifer within the sparging tank (L^3), i.e. 181 L
V_a	total volume of sparged air within the saturated soil (L^3)
V_h	volume of headspace above the sparging tank (L^3), i.e. 18 L
V_w	total volume of water within the saturated porous media (L^3)
v_{sG}	superficial air velocity ($L T^{-1}$), determined as $v_{sG} = Q/As$

Greek letters

μ_L	dynamic viscosity of water ($M L^{-1} T^{-1}$)
ρ_L	density of water ($M L^{-3}$)
τ	air–water interfacial tension ($M L^{-3} T^{-1}$)
μ_G	dynamic viscosity of air ($M L^{-1} T^{-1}$)

They found that in moderate permeable soils (e.g., sandy soil) and at low air injection rates, stable air channels were formed.

Air sparging is expected to increase the rate of volatilization by increasing contact between the contaminants and sparged air. To quantify mass removal, diffusion of contaminants in aqueous phase along with mass-transfer across the air–water interface has been invoked [7–12]. Air–water mass transfer is usually described by a first-order kinetic process as a function of the mass transfer coefficient and air–water interfacial surface area.

In this study, visualization experiments were conducted using a sand box. The type of air flow formed in saturated soil was investigated using X-ray imaging. Air–water mass transfer coefficients were estimated based on the data obtained from a 55-gal sparging tank. Two types of soil, three different VOCs and three injected air flow rates were used for the air sparging experiments. Air–water mass transfer coefficients were determined using a diffusion-based "two-zone model". Finally, a correlation for the air–water mass transfer coefficient was developed and compared with the other studies.

2. Materials and methods

2.1. Air sparging soil tank

Air sparging experiments were conducted using a 55-gal (208 L) polyethylene tank with a diameter of approximately 61 cm and a depth of 89 cm. For each experimental run, the volume and depth of soil packed in the tank were approximately 181 L and 81 cm, respectively. The free water surface was kept at about 2.5 cm above the soil. This experimental setup simulated a typical unconfined aquifer without an unsaturated zone. As shown in Fig. 1, the air injection well was vertically located at the center of the sparging tank. The lower end of the screen for air injection was placed at approximately 5 cm above the bottom of the tank. The sparging screen was a porous stone tube with a diameter of 5 cm and a length of 10 cm. The air sparging experiments were conducted under stagnant water conditions which was reasonable for the laboratory-scale study [7–9].

Two sampling ports each on the influent and the effluent air flow line were used to collect air samples for analysis. Both the influent and effluent air flow lines were monitored by pressure gauges (Ashcroft, AP-14, ±5% accuracy, Stratford, CT) and flow meters (Gilmont, GF-2300, ±2% accuracy, Barrington, IL.). Injected air flow was provided by an oil-free air compressor (DeVilbiss Air Power Co., Jackson, TN). The particulates and oil drops in the injected air flow were removed using a 0.1 μm compressed air filter (Cole Parmer, CZ-02917-00, Vernon Hills, IL.). The flow rates through the system were controlled by a metal

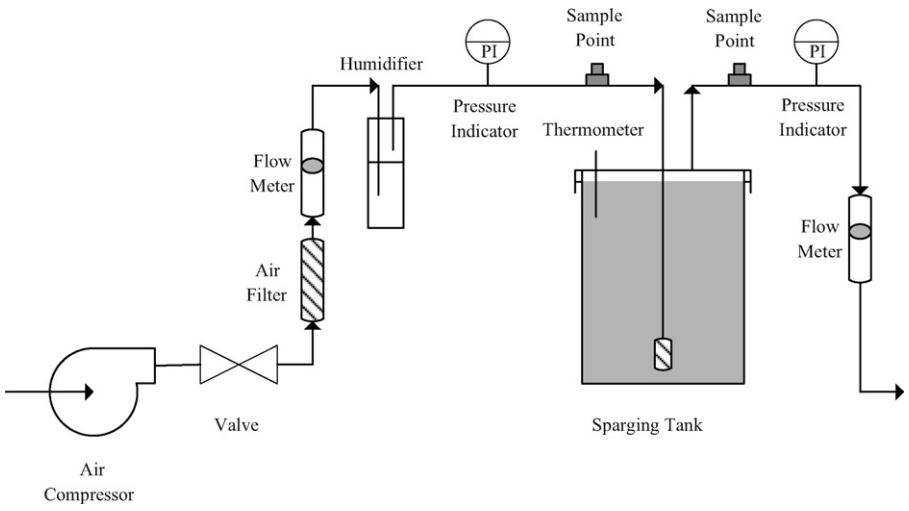

Fig. 1. Sketch of air sparging system.

valve (Cole Parmer, CZ-03218-80, Vernon Hills, IL.). Prior to entering the sparging tank, injected air was saturated with water by passing through a humidifier which consisted of a 0.5-L glass bottle filled with 0.4-L of water. In the air sparging tank, the temperature of porous media was kept at 22 ± 3 °C throughout each experimental run.

The air sparging tank was filled with VOCs aqueous solution and then was sealed. The concentrations of aqueous solution were analyzed to check the losses of VOCs in the sparging tank. The aqueous solutions were sampled using a gas-tight syringe and then immediately injected into a gas chromatograph equipped with a flame ionization detector (Shimadzu, GC/FID-14A, Columbia, MD) and a DB-5 capillary column (J&W, Folsom, CA). Losses of VOCs in the sparging tank were estimated to be less than 6% after 24 h. This also showed that adsorption of VOCs onto the wall of polyethylene tank and diffusion through the tank material would be negligible.

2.2. Materials

Two different types of porous media, coarse sand and fine sand, were used for the air sparging experiments. The properties of porous media used in the experiments are summarized in Table 1. The grain size distribution analyses were determined using the ASTM D422-63 sieving method. The average particle sizes (d_{50}) of coarse sand and fine sand were 1.709 mm and 0.398 mm, respectively. It is noted that the two types of porous media were well-sorted sand. The hydraulic conductivities of coarse sand and fine sand were estimated to be 0.0273 and 0.0549 cm/s using the constant head method. Total carbon content and organic carbon content were determined using the wet combustion method [13].

Table 1
Physical–chemical properties and modeling parameters of porous media

Soil type	Coarse sand	Fine sand
Grain size (mm)	0.42–2.38	0.106–1.0
Average grain size, d_{50} (mm)	1.709	0.398
Uniformity coefficient, d_{60}/d_{10}	1.6	2.2
Porosity	0.410	0.388
Hydraulic conductivity (cm/s)	0.0549	0.0273
Specific density (g/cm^3)	2.891	2.606
Bulk density (g/cm^3)	1.561	1.590
Total carbon content (%)	0.38	0.44
Organic carbon content, f_{oc} (%)	0.30	0.39
Total volume of water, V_w (L)	92.0	79.2
Total mass of porous media, M_s (kg)	283.3	255.4

VOCs used for the experiments were chloroform, TCE and carbon tetrachloride. As given in Table 2, the physical–chemical properties of the three VOCs encompassed a wide range of values. Solubility ranged from 800 mg/L for carbon tetrachloride to 8000 mg/L for chloroform. Henry's constants for the VOCs varied from 0.147 for chloroform to 1.241 for carbon tetrachlo-

Table 2
Physical and chemical properties of VOCs

Compound	Solubility[a] (mg/L)	H[b]	K_{oc}[c] (mL/g)	D_G[d] (cm^2/s)
Trichloroethylene (GC grade, Fluka)	1100	0.397	126	0.082
Chloroform (HPLC grade, Fluka)	8000	0.147	31	0.089
Carbon Tetrachloride (ACS, Aldrich)	800	1.241	110	0.080

Data @ 25 °C.
[a] Solubility @ 20 °C [25].
[b] Henry's constant (dimensionless)[25].
[c] Organic carbon partition coefficient [25].
[d] Diffusion coefficient in gas estimated using the Hirschfelder, Bird and Spotz equation [26].

ride. The three VOCs, purchased from Fluka (Switzerland) and Aldrich (Milwaukee, WI), were of purity greater than 99.5%. Working aqueous solutions of VOCs were prepared by dissolving VOCs in the deionized water. Before the solution was mixed with porous media, the concentrations of aqueous VOCs solutions were 1049, 476 and 476 mg/L for chloroform, TCE and carbon tetrachloride, respectively.

2.3. Visualization of air flow in saturated soil

Visualization experiments were conducted using a sand box (50 cm wide × 50 cm high × 3 cm deep). The sand box was constructed of 5 mm thick Plexiglas as shown in Fig. 2. The soil depth in the box was 40 cm, and a water level of about 5 cm was maintained above the soil. Air was sparged into the saturated soil through a 1.5-cm-diameter diffuser attached to the bottom of the sand box. The saturated soil was packed by transferring the sand slurry layer by layer to minimize trapped air bubbles in the saturated soil. The sand box was then allowed to settle for at least 24 h before air was injected into the soil. The injected air flow rates were approximately 1 and 2 L/min, respectively.

Images of air flow within the saturated soil were scanned using a medical X-ray scanner (Shimadzu ED-125L, Japan) when the desired air flow rate was stabilized. The voltage and tube current of the X-ray scanner were 64–70 kV and 150 mA, respectively, and the duration of X-ray exposure was between 0.07 and 5 s. The size of scanning area was 40 cm × 40 cm on the front wall of the sand box. The distance between the sand box and X-ray scanner was approximately 110 cm. This effort was made to take the X-ray photographs in the same scale of the sand box. The X-ray photographs provided an image of the air flow formed in the saturated soil.

2.4. Experimental procedure of soil tank

The sand used in the experiments was washed thoroughly with clean tap water and any free water drained. The contaminated soil media was made by thoroughly mixing the clean soil with aqueous VOCs solution, and transferred into the sparging tank layer by layer. The initial mass of VOCs in the packed tank, M^o, was determined by the products of the concentrations and volume of aqueous solutions. The packing was completed within 20 min. The procedure ensured that the concentration of VOC throughout the packed tank was fairly uniform. Efforts were taken to minimize volatilization of VOC during the packing as much as possible. The tank was immediately sealed, and the VOC-contaminated soil was allowed to equilibrate for at least 30 h before air was injected into the packed tank.

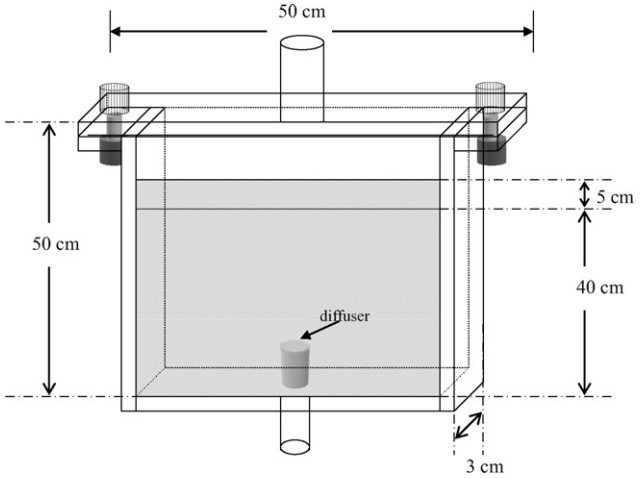

Fig. 2. Dimensions of sand box for visualization experiment.

Three different air flow rates, 20, 35 and 50 L/min, were used for the experiments. After initializing the air sparging experiment, air samples from the effluent sampling port were analyzed every 15 min during the first 12 h, after which air samples were taken hourly. During the sparging experiment, air samples were taken from the influent flow and analyzed to ensure that the injected air was VOC-free. The air samples were taken using a gas-tight syringe and then immediately injected into the GC/FID. The sparging experiments were continuously operated over a 24-h period and were terminated when the VOC concentration in the off-gas was low or remained relatively constant.

At the end of the experimental run, soil and water samples in the air sparging tank were collected. The residual VOC concentrations in the aqueous and soil samples were measured by the GC/FID. Dewatered soil samples were extracted with methanol to determine the amount of VOC in soil [14]. A 1:3 ratio (w/w) mixture of methanol and dewatered soil was vortexed at room temperature for 12 h and then centrifuged at 1240 × g for 30 min. The supernatant was filtered using a syringe filter and was placed in a 1-mL amber glass vial capped with Teflon-faced silicone septa. VOCs in the soil were quantified by direct injection of the supernatant into the GC/FID. Therefore, the total mass of VOCs removed by injected air and remained in the sparging tank was determined. The difference of VOCs mass balances between initial and after air sparging experiments was found to be less than 10%, which possibly resulting from mass lost during the packing.

3. Results and discussion

3.1. Images of air flow in saturated soil

As shown in Fig. 3, the air flow, illustrated as dark area in the X-ray photographs, was in the form of bubbles for the coarse sand (d_{50} = 1.709 mm). On the other hand, Fig. 4 shows the sparged air in the fine sand (d_{50} = 0.398 mm) most probably flowed in different air channel sizes. The air flow moved upward forming a cone-like air plume and remained in this stable pattern. As shown in Figs. 3 and 4, the shape and size of the air plume were similar for the two different air flow rates.

In Fig. 3(b), the X-ray photograph for 2 L/min showed more dark images than the flow rate of 1 L/min, which implying that the volume of sparged air in the saturated coarse sand increased with air flow rate. However, the change in the number and sizes of the bubbles was not clear for the two flow rates. Also seen in Fig. 4, discrete air channels formed in the fine sand and with an increase in the air flow rate, the more dark images were observed in Fig. 4(b). This indicated that new air channels were formed

within the air plume. In addition, the sizes of the air channels were found to be larger for the higher flow rate.

In the laboratory study of air sparging, Ji et al. [15] indicated that there were two distinct air flow regimes in water saturated glass beads over a range of air injection pressures. For grain sizes of 0.75 mm or less, the air flow was observed to be in the form of pore-scale air channels. Similar results were found in the fine sand (d_{50} = 0.398 mm) of this study. Ji and his coworkers also showed that with 2 mm glass beads, both air channels and bubbly flow were observed. However, Fig. 3 indicated that air flow may occur as discrete bubbles for the coarse sand (d_{50} = 1.709 mm).

As flowing through the porous media, pressurized air will preferentially enter the pores with the smallest capillary pressure [16]. It is known that the capillary pressure is inversely proportional to the radius of curvature of the air–water interface. For a sandy aquifer, the radius of curvature of the interface is dependent on the grain size as well as grain sharp. Therefore, in an air sparging system, it is speculated that the type of air flow will depend on the size and sharp of porous media. This can be one of the possible reasons that the air bubbles formed in the coarse sand herein, which differing from the study of Ji et al. [15].

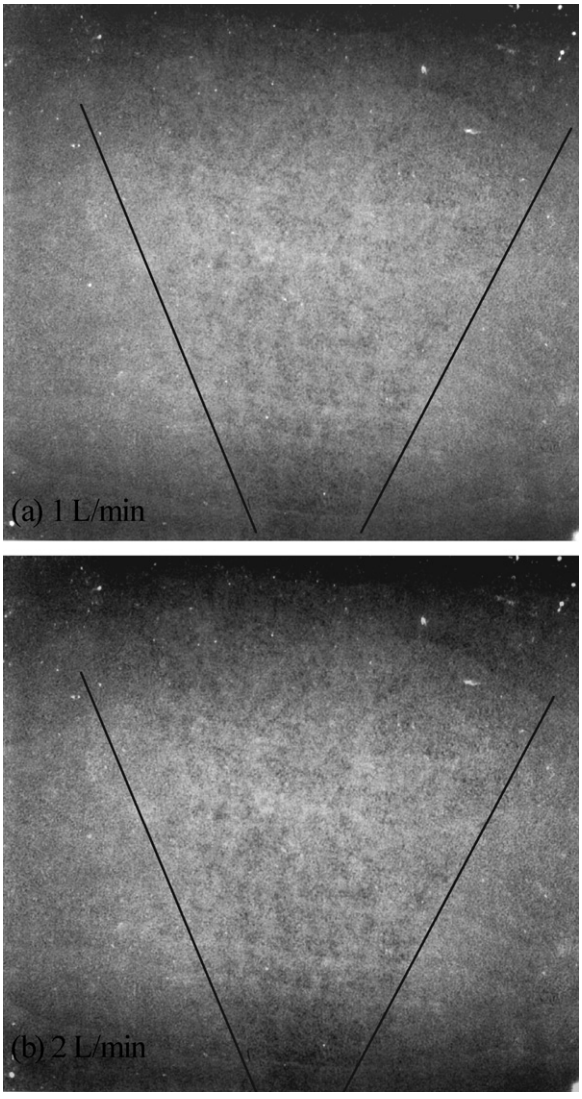

Fig. 3. X-ray photographs of coarse sand under air sparging conditions. (The air bubbles illustrated as dark area were formed within the cone-like area. The size of original X-ray photograph was 40 cm × 40 cm.)

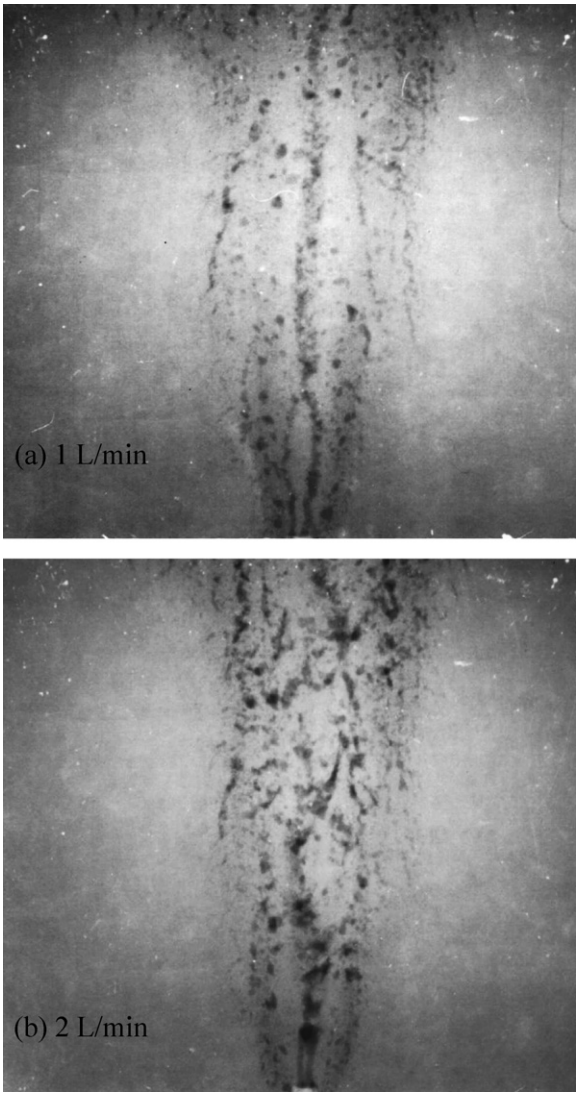

Fig. 4. X-ray photographs of fine sand under air sparging conditions. (Air was flowed in different sizes of channels within the cone-like air plume. The size of original X-ray photograph was 40 cm × 40 cm.)

3.2. Results of air sparging tank

Fig. 5 presents typical experimental results showing the change in effluent air concentrations of VOCs with time for the 55-gal air sparging tank experiments using fine and coarse sand. Initial injection of air through the saturated porous media resulted in a rapid decrease in the VOCs concentrations in the effluent air. After that, the air concentrations decreased slowly and approached an asymptotic value, implying a quasi-steady condition for the volatilization of VOCs was reached. This low concentration continued until an undetectable value was reached after a period of sparging time.

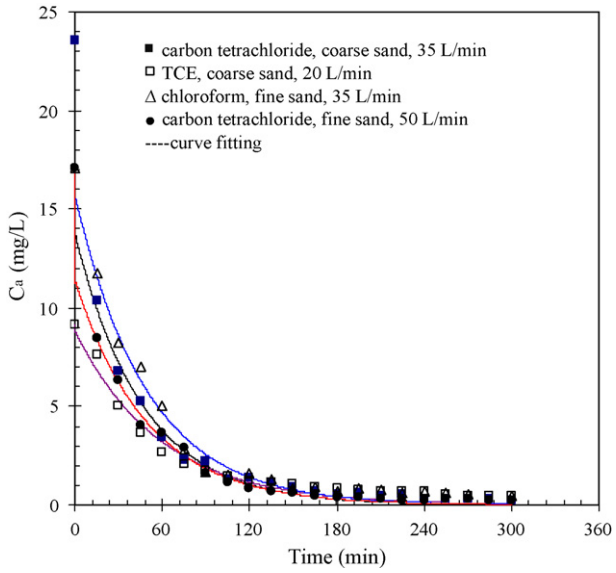

Fig. 5. Experimental results for air sparging experiments.

3.3. Two-zone model

The two-zone model has been proposed to estimate the air–water mass transfer coefficients for bench-scale air sparging experiments [7–9,11,17]. As shown in Fig. 6, air flow within the porous media is assumed to be in the form of air channels. The effects of air compressibility and holdups are assumed to be negligible. A continuous film of water is assumed to exist between the air channels and the soil particles. When VOCs are volatilized from the air–water interface, VOCs in the bulk water away from the air–water interface will diffuse to the air–water interface due to a concentration gradient. Therefore, under air sparged conditions, a certain fraction of the saturated porous media may be assumed to be the "mass transfer zone" (MTZ). Because of the low aqueous diffusivity of VOCs, the "bulk media zone" may be assumed to be unaffected by the air channels. Air–water mass transfer occurs between the air channels and the MTZ.

Since the MTZ is directly affected by the air channels, a fraction F may be defined to account for the volume of the MTZ to the total volume of the saturated porous media. The fraction F is a function of the size of the air channels, the distance between two air channels and probably the aqueous-phase diffusivity of the VOC. Obviously, the larger the average distance between two air channels, the lower will be the F value. Under such circumstances, less volume of the porous media will be affected by the air channels.

In the MTZ, the mass transfer rate, J, of VOCs between air and water phases is modeled using a first order kinetic process as follows:

$$J = K_{\mathrm{G}}\mathrm{A}(HC_{\mathrm{wm}} - C_{\mathrm{a}}) \tag{1}$$

Under constant air flow conditions, the overall mass balance for the advecting air phase of an air sparging system is given as follows:

$$V_{\mathrm{a}}\frac{\mathrm{d}C_{\mathrm{a}}}{\mathrm{d}t} = K_{\mathrm{G}}\mathrm{A}(HC_{\mathrm{wm}} - C_{\mathrm{a}}) - QC_{\mathrm{a}} \tag{2}$$

Sorption between the soil and water phases is assumed to be at equilibrium, and the partitioning process is described by a linear isotherm [18]. The mass balance equation for the MTZ can be described as:

$$F(M_{\mathrm{s}}K_{\mathrm{p}} + V_{\mathrm{w}})\frac{\mathrm{d}C_{\mathrm{wm}}}{\mathrm{d}t} = K_{\mathrm{G}}\mathrm{A}(C_{\mathrm{a}} - HC_{\mathrm{wm}}) \tag{3}$$

As shown in Table 1, the organic carbon content, f_{oc} (%), of coarse sand and fine sand were greater than 0.1%. The soil–water partition coefficient, K_{p}, can be determined by the organic carbon partitioning coefficient, K_{oc}, as $K_{\mathrm{p}} = f_{\mathrm{oc}}K_{\mathrm{oc}}$ [19]. Since the total air–water interfacial area of air channels cannot be determined, K_{G} and A are lumped together as the mass transfer coefficient, $K_{\mathrm{G}}\mathrm{A}$. It is obvious that F cannot be predicted a priori. Therefore, $K_{\mathrm{G}}\mathrm{A}$ and F were estimated by curve fitting the model to the experimental data using least-squares analysis.

In this study, the concentrations C_{a} and C_{wm} were determined using the analytical solutions of Eqs. (2) and (3). The initial VOCs concentrations in the sparged air were determined experimentally as follows:

$$C_{\mathrm{a}}^{\mathrm{o}} = C_{\mathrm{a,experimental}}^{\mathrm{o}} \tag{4}$$

By taking the mass balance for the sparging tank, the initial average VOCs concentration in water of the MTZ was estimated

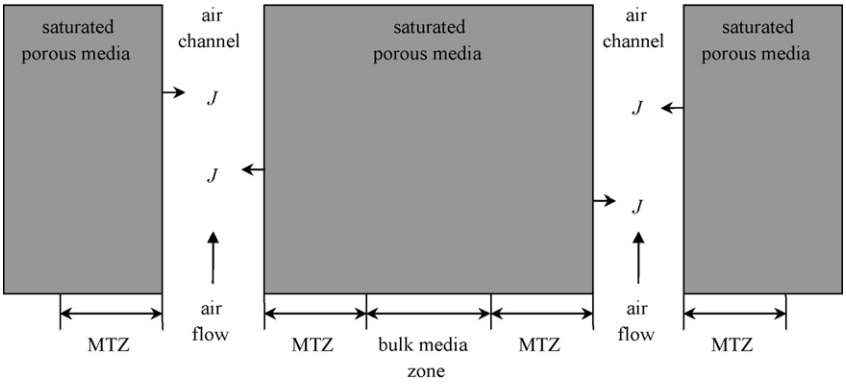

Fig. 6. Conceptual picture of the two-zone air sparging model.

Table 3
Volume of sparged air within the saturated soil

Air flow rate (L/min)	Volume of Air within the aquifer[a], V_a (L)	
	Coarse sand (d_{50} = 1.709 mm)	Fine sand (d_{50} = 0.398 mm)
20	0.514	0.427
35	0.779	0.596
50	1.173	0.970

[a] V_a was estimated using the water displacement method.

as follows:

$$C^{o}_{wm} = \frac{M^{o} - V_h C^{o}_{a}}{(M_s K_p + V_w)} \quad (5)$$

The modeling parameters for the experiments are given in Tables 1 and 2. During air sparging experiments, the air channels or bubbles displaced the pore water in saturated soil. It was impossible to directly determine the total volume of sparged air within the aquifer. For a modeling purpose, V_a was assumed to equal to the increase of free water above the aquifer. As presented in Table 3, V_a was indirectly estimated using the water displacement method.

In most engineering cases, it is customary to report the air–water mass transfer coefficient, $K_G a$ (T^{-1}), which is a product of the overall gas-phase mass transfer coefficient and the air–water interfacial surface area per unit volume of the mass transfer system. In this study, $K_G a$ was obtained as [7]:

$$K_G a = \frac{K_G A}{V} \quad (6)$$

As shown in Fig. 5, the two-zone model curve-fitted well the experimental data. The estimated $K_G a$ and F values are summarized in Table 4. The magnitudes of $K_G a$ values obtained were between 10^{-2} and 10^{-3} 1/min, and F values were ranged 0.203–0.54. For all experimental matrix, the experimentally measured VOCs concentrations were found to be significantly correlated to the results of curve-fitting with $R^2 = 0.993$ ($p < 0.001$). Fig. 7 shows a sensitivity analysis for the two-zone model. For carbon tetrachloride sparged from the coarse sand, the estimated $K_G a$ and F values are 0.014 (1/min) and 0.54, respectively. With a slight change in $K_G a$ or F, the simulated VOCs concentrations in the effluent air were obviously diverged from the experimental results.

Although the two-zone model is based on the assumption of sparged air moving in channels, the simulation results indicate that this model can also be used for air bubbles flow which was seen in the coarse sand of this study. In the two-zone model, the effect of air flow type on mass transfer can be lumped into parameter F. Under air sparging conditions, it is reasonable to assume a bulk media zone that is not in contact with the air channels or bubble flow. Results of laboratory experiments [7–9] and field study [20] have supported this hypothesis.

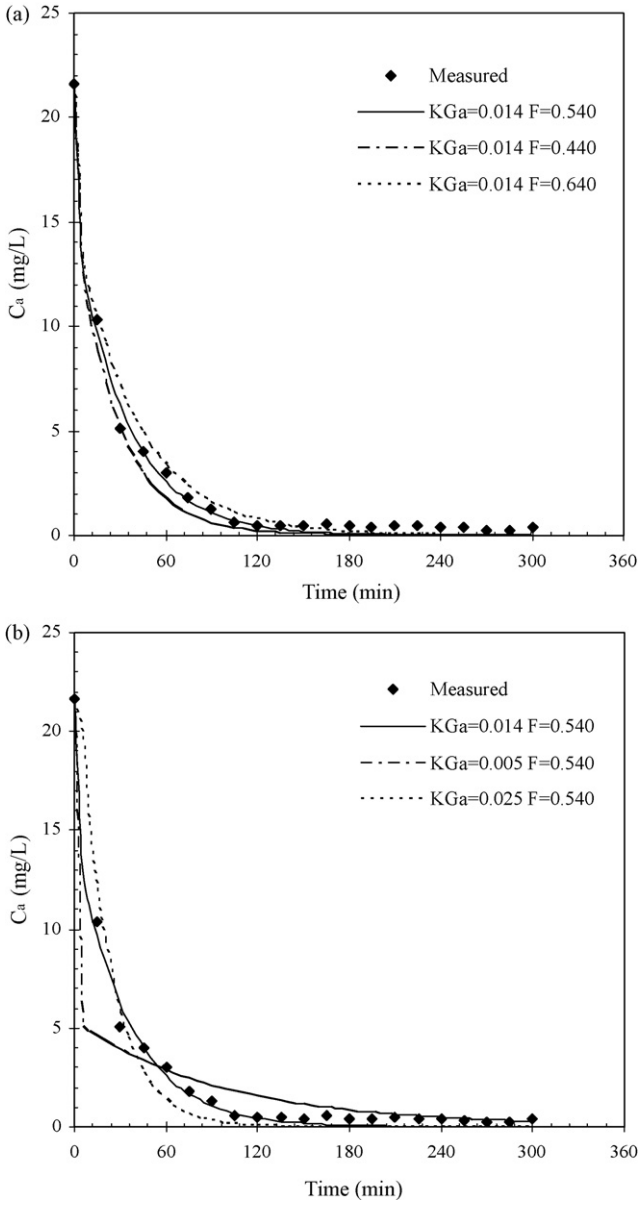

Fig. 7. Sensitivity analysis for carbon tetrachloride sparged in coarse sand.

Table 4
$K_G a$ and F for the air sparging experiments

Flow rate (L/min)	Coarse sand				Fine sand			
	TCE		Carbon tetrachloride		Chloroform		Carbon tetrachloride	
	$K_G a$	F	$K_G a$	F	$K_G a$	F	$K_G a$	F
20	0.012	0.238	0.003	0.204	0.016	0.212	0.002	0.203
35	0.018	0.309	0.009	0.478	0.021	0.234	0.004	0.296
50	0.029	0.435	0.014	0.540	0.027	0.287	0.011	0.464

$K_G a$ (1/min).

From the X-ray image of sand box experiments, it was observed that the volume of air bubbles as well as the sizes and numbers of the air channels were proportional to the air flow rates for coarse sand and fine sand, respectively, which in turn may result in a larger air–water interfacial surface area for mass transfer and more volume for MTZ. As presented in Table 4, the values of K_Ga and F were estimated to be proportional to the air flow rates.

For carbon tetrachloride, K_Ga's obtained in coarse sand were greater than fine sand at the same air flow rate. This may be due to the larger total surface area of air bubbles formed in the coarse sand than that of air channels in fine sand during air sparging, or the possibility of fluid agitation due to air bubbles [2], which may result in a greater fraction of aquifer being affected by air bubbles.

3.4. Correlation of mass transfer coefficient

The estimated K_Ga values were correlated against the various physical–chemical properties of the air sparging experiments and conditions. Dimensionless parameters such as Peclet number *Pe*, Sherwood number *Sh* and normalized mean particle size d_o have been proposed to quantify the air–water mass transfer in porous media [7–9,21,22]. These dimensionless parameters are defined as follows:

$$Sh = \frac{K_G a (d_{50})^2}{D_G} \tag{7}$$

$$Pe = \frac{v_{sG} d_{50}}{D_G} \tag{8}$$

$$d_o = \frac{d_{50}}{d_m} \tag{9}$$

The Sherwood number characterizes the relationship between air–water mass transfer and gaseous phase diffusion. The Peclet number is the ratio of advection to diffusion of the gaseous phase and may represent the dimensionless air flow rate. In the present work, K_Ga was incorporated into the dimensionless Sherwood number and was correlated with the Peclet number, Henry's constant and the normalized mean particle size. Multiple linear regression analyses were performed to determine the best fit model parameters a_i for the log-linearized form of the empirical correlation:

$$\log(Sh) = \log a_o + a_1 \log(Pe) + a_2 \log(d_o) + a_3 \log(H) \tag{10}$$

The importance of each dimensionless number was determined from the single-parameter model analyses. Henry's constant was correlated to the Sherwood number only with $R^2 = 0.007$ ($p = 0.796$). The Sherwood number was significantly correlated to the normalized mean particle sizes d_o ($R^2 = 0.785$, $p < 0.001$) and Peclet number ($R^2 = 0.774$, $p < 0.001$). The correlation results imply that the air–water mass transfer coefficient K_Ga was strongly affected by the particle size of porous media and the air flow rates. Similar results were found in the air sparging soil column study of Chao et al. [7] as well as Braida and Ong [8].

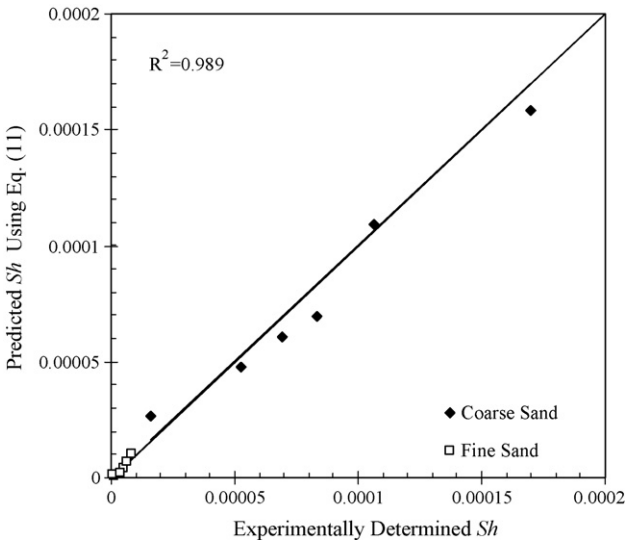

Fig. 8. Comparison of experimentally determined Sherwood numbers with predicted Sherwood numbers.

The empirical dimensionless correlation of Eq. (10) was obtained as follows ($R^2 = 0.957$, $p < 0.001$):

$$Sh = 10^{-4.54} Pe^{1.05} d_o^{1.27} H^{-0.74} \tag{11}$$

Comparison of the empirical model predictions and estimated Sherwood numbers is presented in Fig. 8, indicating that the estimated Sherwood number can be accurately represented using Eq. (11). According to Eq. (11), K_Ga can be further expressed as:

$$K_G a = 10^{-2.89} \left(\frac{Q}{A_s}\right)^{1.05} D_G^{-0.05} d_{50}^{0.32} H^{-0.74} \tag{12}$$

3.5. Comparison of other correlations

Wilkins et al. [21] conducted several SVE soil column experiments to investigate volatilization of NAPLs in unsaturated sandy porous media. They used the same dimensionless parameters of this study and developed a correlation for NAPL–air mass transfer as follows:

$$Sh = 10^{-2.79} Pe^{0.62} d_o^{1.82} \tag{13}$$

Fig. 9 shows the comparison of Sherwood numbers for carbon tetrachloride obtained in this study with those calculated from the Wilkins et al. correlation of Eq. (13). As presented in Fig. 9, Sherwood numbers from this study were approximately 100 times lower than the predicted results of the Wilkins et al. correlation. The higher Sherwood numbers predicted by the Wilkins et al. correlation may be due to the presence of NAPLs which would directly volatilize into the air phase. Therefore, the NAPL–air mass transfer correlation of Wilkins et al. may not only represent mass transfer between air and water phases but also NAPL–air interphase mass transfer. Additionally, in the unsaturated zone a larger fraction of the soil matrix can be exposed to the advecting air stream and therefore, the available

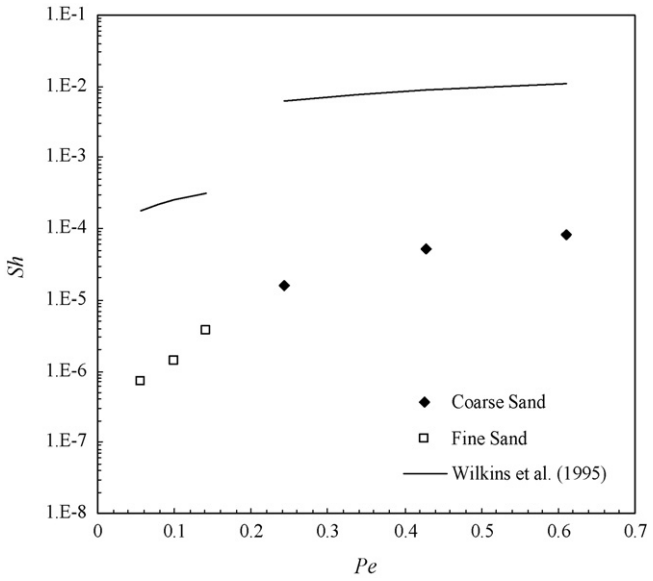

Fig. 9. Experimentally measured Sherwood numbers for carbon tetrachloride and correlation of Wilkins et al. [21].

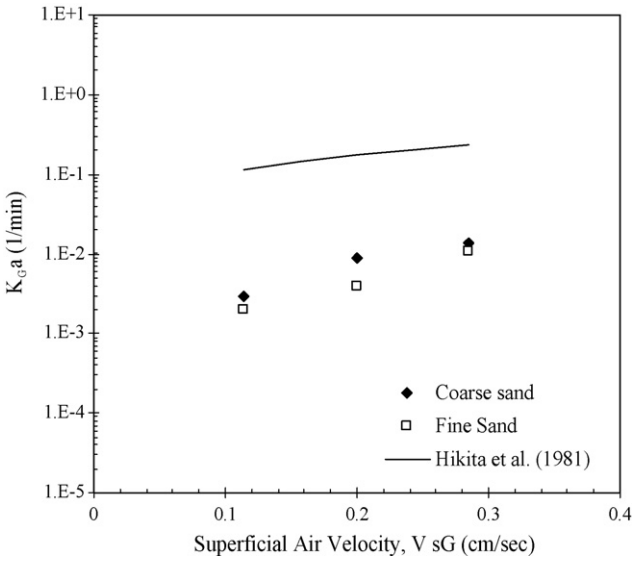

Fig. 10. Comparison of experimentally measured $K_G a$ for carbon tetrachloride with correlation of Hikita et al. [23].

total air–water interfacial area during soil venting conditions was much higher than air sparging. The mass transfer coefficient obtained from the correlation of Wilkins et al. would be expected to be higher than the work presented here.

Hikita et al. [23] investigated the liquid-phase mass transfer coefficient, $k_L a$ (T^{-1}), for the bubble aeration column, and the air–water mass transfer correlation was given as:

$$K_L a = 14.9\left(\frac{v_{sG}\mu_L}{\tau}\right)^{1.76}\left(\frac{\mu_L g}{\rho_L \tau^3}\right)^{-0.248}\left(\frac{\mu_G}{\mu_L}\right)^{0.243} \times \left(\frac{\mu_L}{\rho_L D_L}\right)^{-0.604} \quad (14)$$

For VOCs with high Henry's constant ($H > 0.1$), $K_G a$ can be determined as: $K_G a = k_L a/H$ [24]. Fig. 10 compares the values of $K_G a$ for carbon tetrachloride obtained in this study with those for a bubble column aeration system of carbon tetrachloride contaminated water. The $K_G a$ values for bubble column aeration were computed using the correlation of Eq. (14). In Fig. 10, it can be seen that $K_G a$ values predicted by the correlation of Hikita et al. were approximate one order of magnitude larger than the $K_G a$'s obtained in this study.

In a bubble aeration column, air–water mass transfer occurs across the interfacial surface of numerous air bubbles. The total surface area of air bubbles formed in the bubble column can be much greater than that of the air bubbles or channels formed in the aquifer during air sparging. Even if air bubbles were formed in the coarse sand of this study, the porous media itself served as a barrier in retarding the movement of VOCs from the aqueous phase to the air–water interface.

Chao et al. [7] conducted a bench-scale soil column with a depth of 12 in. (30.5 cm) to investigate the nonequilibrium mass transfer of VOCs under air sparging conditions and obtained the following empirical dimensionless correlation:

$$Sh = 10^{-4.71} Pe^{0.84} d_o^{1.71} H^{-0.61} \quad (15)$$

Trends represented as Eq. (15) were consistent with the empirical correlation of Eq. (11) obtained in this study. Fig. 11 shows that the Sherwood numbers predicted using the empirical correlation of Eq. (15) were significantly correlated ($R^2 = 0.975$, $p < 0.001$) to the experimental Sherwood numbers of this study. Also seen in Fig. 11, the results were very close to 1:1 line indicating an excellent agreement between the empirical correlation of Chao et al. and the estimated $K_G a$ values as shown in Table 4. Under air sparging conditions, the air–water mass transfer coefficient of VOCs could be estimated using the two-zone model and quantified by the mass transfer correlation of Eq. (11).

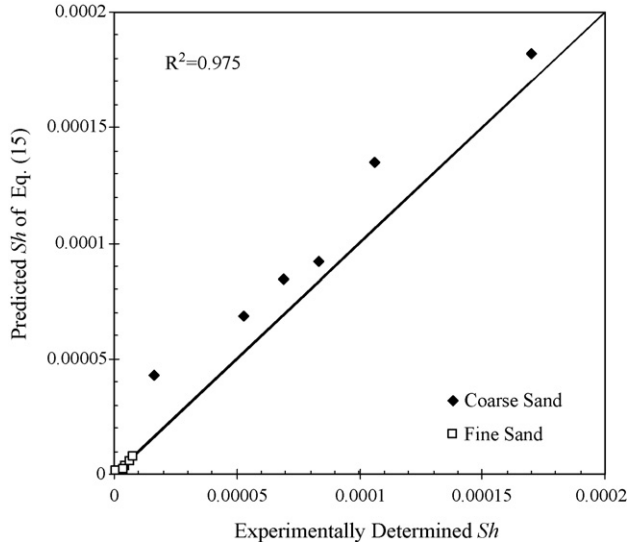

Fig. 11. Comparison of experimentally determined Sherwood numbers with predicted Sherwood numbers using Eq. (15).

4. Conclusion

From the X-ray images of an air sparging sand box, the air flow was observed to be in the form of air bubbles or air channels depending on the particle size of porous media. The size and number of air channels were found to increase with air flow rates in the fine sand, while not much significant differences in bubble sizes were observed in the coarse sand. A one-dimensional lumped parameter model was proposed to estimate the air–water mass transfer coefficient for a 55-gal air sparging tank. In this model, nonequilibrium mass transfer of VOCs between air and water phases was modeled using a first order kinetic process, and VOCs in the water phase were modeled by assuming that there were two zones in the porous media. The two zones were: the mass transfer zone in which VOCs were transferred from the water phase to the air phase and were affected by air sparging while the other zone was the bulk media zone where air flow had no direct impact on mass transfer. The modeling results imply that the two-zone model could be appropriate for sparged air flow formed in either bubbles or channels.

The experimental air–water mass transfer coefficients obtained from this study ranged from 10^{-2} to 10^{-3} 1/min. A correlation for the air–water mass transfer coefficient was developed using Sherwood number, Peclet number, Henry's constant and the mean particle size of porous media. The experimental air–water mass transfer coefficients obtained from this study were much smaller than that for the bubble aeration column and SVE systems. Under the conditions of an immobile water phase, the air–water mass transfer coefficients were found to be proportional to the air flow rates and the mean particle size of porous media but were inversely proportional to the Henry's constant. The air–water mass transfer correlation done herein can be the fundamental work for further study on the volatilization of VOCs during air sparging system.

Acknowledgment

The study was partially supported by the National Science Council, Taiwan, ROC (NSC92-2622-E-039-001-CC3).

References

[1] P. Johnson, Assessment of the contributions of volatilization and biodegradation to in situ air sparging performance, Environ. Sci. Technol. 32 (2) (1998) 276–281.
[2] W. Ji, A. Dahmani, D. Ahlfeld, J.D. Lin, E. Hill, Laboratory study of air sparging: air flow visualization, Ground Water Monit. Rem. 13 (4) (1993) 115–127.
[3] J. Peterson, K. Murray, Y. Tulu, B. Peuler, D. Wilkens, Air-flow geometry in air sparging of fine-grained sands, Hydrogeology J. 9 (2) (2001) 168–176.
[4] M.C. Marley, D.J. Hazebrouck, M.T. Walsh, The application of in-situ air sparging as an innovative soils and groundwater remediation technology, Ground Water Monit. Rem. 12 (2) (1992) 137–145.
[5] R.E. Hinchee, Air sparging state of the art, in: R.E. Hinchee (Ed.), Air Sparging, Lewis Publishers, Boca Raton, FL, 1994, pp. 1–13.
[6] J.F. Pankow, R.L. Johnson, J.A. Cherry, Air sparging in gate wells in cutoff walls and trenches for control of plumes of volatile organic compounds (VOCs), Ground Water 13 (4) (1993) 654–663.
[7] K.P. Chao, S.K. Ong, A.L. Protopapas, Water-to-air mass transfer of VOCs: laboratory-scale air sparging system, J. Environ. Eng. ASCE 124 (11) (1998) 1054–1060.
[8] W.J. Braida, S.K. Ong, Air sparging: air-water mass transfer coefficients, Water Resour. Res. 34 (12) (1998) 3245–3253.
[9] W.J. Braida, S.K. Ong, Modeling of air sparging of VOC-contaminated soil column, J. Contam. Hydrol. 41 (2000) 385–402.
[10] J.E. McCray, Mathematical modeling of air sparging for subsurface remediation: state of the art, J. Hazard. Mater. 72 (2000) 237–263.
[11] S.W. Rogers, K.P. Chao, S.K. Ong, Benzene nonaqueous phase liquids removal under air-sparged conditions, J. Environ. Eng. ASCE 130 (7) (2004) 751–758.
[12] M.E. Rahbeh, R.H. Mohtar, Application of multiphase transport models to field remediation by air sparging and soil vapor extraction, J. Hazard. Mater. 143 (2007) 156–170.
[13] L.E. Allison, Wet-combustion apparatus and procedure for organic and inorganic carbon in soil, Soil Sci. Soc. Am. Proc. 24 (1960) 36–40.
[14] S.G. Pavlostahis, G.N. Mathavan, Desorption kinetics of selected volatile organic compounds from field contaminated soils, Environ. Sci. Technol. 26 (3) (1992) 532–538.
[15] W. Ji, A. Dahmani, D. Ahlfeld, J.D. Lin, E. Hill, Laboratory study of air sparging: air flow visualization, Ground Water Monit. Rem. 13 (4) (1993) 115–126.
[16] J. Bear, Dynamics of Fluids in Porous Media, America Elsevier, New York, NY, 1972.
[17] W.J. Braida, S.K. Ong, Air sparging effectiveness: laboratory characterization of air-channel mass transfer zone for VOC volatilization, J. Hazard. Mater. 87 (2001) 241–258.
[18] M.L. Brusseau, Factors influencing the transport and fate of contaminants in the subsurface, J. Hazard. Mater. 32 (1992) 137–143.
[19] S.W. Karickhoff, Organic pollutant sorption in aquatic systems, J. Hydraulic Eng. ASCE 110 (1984) 707–735.
[20] A.J. Rabideau, J.M. Blayden, C. Ganguly, Field performance of air-sparging system for removing TCE from groundwater, Environ. Sci. Technol. 33 (1) (1999) 157–162.
[21] M.D. Wilkins, L.M. Abriola, K.D. Pennell, An experimental investigation of rate-limited nonaqueous phase liquid volatilization in unsaturated porous media: steady state mass transfer, Water Resour. Res. 31 (9) (1995) 2159–2172.
[22] S.E. Powers, L.M. Abriola, W.J.W. Weber, An experimental investigation of nonaqueous phase liquid dissolution in saturated subsurface systems: Transient mass transfer rates, Water Resour. Res. 30 (2) (1994) 321–332.
[23] H. Hikita, S. Asai, K. Tanigawa, K. Segawa, M. Kitao, The volumetric liquid-phase mass transfer coefficient in bubble columns, Chem. Eng. J. 22 (1981) 61–69.
[24] D. Mackay, W.Y. Shiu, R.P. Sutherland, Determination of air-water Henry's law constants for hydrophobic pollutants, Environ. Sci. Technol. 13 (3) (1979) 333–337.
[25] M.D. LaGrega, P.L. Buckingham, J.C. Evans, Hazardous Waste Management, McGraw-Hill Inc., New York, NY, 1994.
[26] J.R. Welty, C.E. Wicks, R.E. Wilson, Fundamentals of Momentum, Heat and Mass Transfer, John Wiley & Sons Inc., New York, NY, 1984.